Diverging conductance at the contact between random and pure quantum XX spin chains

Christophe Chatelain

Diverging conductance at the contact between random and pure quantum XX spin chains

Christophe Chatelain

Groupe de Physique Statistique, Département P2M, Institut Jean Lamour (CNRS UMR 7198), Université de Lorraine, France

E-mail: christophe.chatelain@univ-lorraine.fr

Abstract. A model consisting in two quantum XX spin chains, one homogeneous and the second with random couplings drawn from a binary distribution, is considered. The two chains are coupled to two different non-local thermal baths and their dynamics is governed by a Lindblad equation. In the steady state, a current J is induced between the two chains by coupling them together by their edges and imposing different chemical potentials μ to the two baths. While a regime of linear characteristics J versus $\Delta\mu$ is observed in the absence of randomness, a gap opens as the disorder strength is increased. In the infinite-randomness limit, this behavior is related to the density of states of the localized states contributing to the current. The conductance is shown to diverge in this limit.

PACS numbers: 05.10.-a, 05.30.-d, 05.30.Fk, 05.60.Gg

1. Introduction

Disorder can have drastic consequences, especially in low-dimensional systems. At thermal equilibrium, the case of the quantum Ising chain in a transverse field has been particularly studied. At the quantum phase transition of the model, the introduction of random couplings leads to a new critical behavior governed by a new infinite-randomness fixed point [1, 2]. Even outside the critical point, in the so-called Griffiths phases, rare disorder configurations induce singularities of the free energy, as well as anomalous dynamical properties [3].

Much less is known about open random spin chains. In this work, we are interested in transport properties of a random spin-1/2 XX chain. Usually, a non-equilibrium steady state (NESS) is induced by coupling two different baths to the two edges of the chain. As in the pure case [4], a non-uniform magnetization profile is expected in the NESS. Since the XX chain can be mapped onto a free fermion gas, the system can be seen as a tight-binding model with random couplings and coupled to two thermal baths with different temperatures and/or different chemical potentials. In the absence of disorder, a uniform current is expected to flow through out the system. Because the eigenmodes of a translation-invariant Hamiltonian are delocalized over the whole chain, the conduction is ballistic. Any excitation created by one bath reaches the second one. The conductivity is therefore infinite, though the conductance is finite and quantized [5, 6, 7]. In contrast, in the presence of randomness, the excitations are

scattered on the impurities so that the conduction becomes diffusive as the disorder is increased. In one-dimensional systems, the consequence is even more drastic because all eigenstates of the Hamiltonian are localized, even with an infinitesimal disorder. Therefore, the excitations cannot propagate from one bath to the other. The current dies off exponentially over the so-called Anderson localization length. The chain is an insulator [8, 9, 10]. This mechanism of localization is preserved when interactions between the charge carriers are considered, i.e. in the so-called Many-Body Localization phase [11].

The coupling with a bath requires some approximations. The simplest one is to consider two semi-infinite chains initially prepared in different thermal states. The two chains are then coupled together and the whole system is considered as isolated in the calculation of its time evolution. In the long-time limit, the magnetization profile $m(x,t)$ is a function of x/t and becomes flat for both XX [4] and XXZ [12] chains. The coupling of a XX chain with two baths at its edges was later taken into account by repeatedly bringing thermalized spins in contact with the system during short time steps [13]. A different route is provided by the Lindblad equation [14, 15]

$$\frac{d\rho}{dt} = -\frac{i}{\hbar}[H,\rho] + 2D[\rho] \tag{1}$$

which gives the effective time evolution of the system in the Markovian and rotating-wave approximations. ρ is the reduced density matrix of the chain and the dissipator $D[\rho]$ has the general structure

$$2D[\rho] = \sum_{\alpha} \gamma_\alpha(t)\Big[V_\alpha(t)\rho(t)V_\alpha^+(t) - \frac{1}{2}\{V_\alpha^+(t)V_\alpha(t),\rho_S(t)\}\Big]. \tag{2}$$

When a bath is coupled only to an edge of the chain, the two only possible Lindblad operators V_α are the ladder operators σ_1^-, σ_1^+ at the left boundary and σ_L^-, σ_L^+ at the right one. Exact results are known for this configuration for the pure XX chain [16]. It was later shown that the steady state of the Lindblad equation admits a representation in terms of Matrix Product State for both the XX [17] and the XXZ [18] chains. In molecular nanowires for which the dynamics of electrons is well described by a tight-binding model, a third reservoir coupled to all sites of the chain is often introduced to describe phase-breaking processes, mainly due to electron-phonon coupling [19]. Such a dephasing effect was also studied for the XX chain by introducing a Lindblad operator σ_i^z coupled to all sites i of the chain [20, 21]. Interestingly, the mechanism of Anderson localization may be avoided with such a bath because the phase decoherence is destroyed [22].

In this study, a random XX chain coupled to delocalized degrees of freedom acting, not only as a thermal bath, but also as a reservoir in the fermion picture, is considered. The coupling is implemented in the Lindblad equation using the phenomenological non-local dissipator recently introduced by Guimarães *et al.* [23]. In the first section, the model is discussed and the dissipator implementing the coupling with the baths is introduced. In the second section, the case of two homogeneous subchains is studied as a preliminary. The conductance, not considered in [23], is computed in the limit of a weak interchain coupling. In the third section, the case of a random left subchain is considered. A divergence of the conductance as the disorder strength increases is observed in the numerical simulations and explained in the infinite-randomness limit. Conclusions follow.

2. Description of the model

We consider an open spin-1/2 XX chain governed by the Hamiltonian

$$H = -\frac{1}{2}\sum_{n=1}^{L-1} J_n(\sigma_n^x\sigma_{n+1}^x + \sigma_n^y\sigma_{n+1}^y) - \sum_{n=1}^{L} h_n\sigma_n^z. \tag{3}$$

The Jordan-Wigner transformation maps the XX chain onto a fermionic tight-binding model, whose Hamiltonian is, up to a constant,

$$H = -\sum_{n=1}^{L-1} J_n(c_n^+c_{n+1} + c_{n+1}^+c_n) - 2\sum_{n=1}^{L} h_n c_n^+c_n \tag{4}$$

where the exchange couplings J_n play the role of hopping constants between nearest-neighboring sites and the transverse fields h_n of a chemical potential. Such a model is relevant for the description of conduction in polymers as polyaniline [24]. In the homogeneous case, i.e. $J_n = J$ and $h_n = h$, the unitary transformation

$$\eta_k = \sum_{n=1}^{L} U_{k,n}c_n = \sqrt{\frac{2}{L+1}}\sum_{n=1}^{L} \sin\frac{nk\pi}{L+1}\, c_n, \quad (k = 1\dots L) \tag{5}$$

diagonalizes the Hamiltonian:

$$H = \sum_{k=1}^{L} \varepsilon_k \eta_k^+\eta_k \tag{6}$$

with the dispersion law $\varepsilon_k = -2J\cos\frac{\pi k}{L+1} - 2h$ $(k = 1, \dots, L)$.

Two such XX chains are joined together to form a single chain of length $2L$. In the right subchain, the couplings are homogeneous, $J_n = 1$, while in the left one, they are random variables drawn from the binary distribution

$$\wp(J_n) = \frac{1}{2}\delta\big(J_n - r\big) + \frac{1}{2}\delta\big(J_n - 1/r\big). \tag{7}$$

This particular choice is motivated by the fact that it allows for the numerical computation of average quantities over all disorder configurations so that the contribution of rare events is properly taken into account. For a left subchain of L sites, the number of random couplings is indeed $L-1$ so that the number of disorder configurations is 2^{L-1}. A Jordan-Wigner transformation is performed independently in each subchain, leading to two species of fermions $c_{\alpha,n}$ $(\alpha = 1, 2)$. The resulting tight-binding Hamiltonian is diagonalized and new fermionic operators $\eta_{\alpha,k}$, annihilating a particle in the k-th eigenmode of the subchain α, are introduced. The right subchain being homogeneous, the unitary transformation between $c_{2,n}$ and $\eta_{2,k}$ is given by Eq. (5). For the left subchain, the unitary transformation

$$\eta_{1,k} = \sum_{n=1}^{L} V_{k,n}c_{1,n} \tag{8}$$

is determined numerically for each disorder realization $\{J_n\}$. The left and right subchains are then connected by a coupling g. The full Hamiltonian reads

$$\begin{aligned} H = & -\sum_{n=1}^{L-1} J_n(c_{1,n}^+c_{1,n+1} + c_{1,n+1}^+c_{1,n}) - g(c_{1,L}^+c_{2,1} + c_{2,1}^+c_{1,L}) \\ & -\sum_{n=1}^{L-1}(c_{2,n}^+c_{2,n+1} + c_{2,n+1}^+c_{2,n}). \end{aligned} \tag{9}$$

No transverse field has been included since the chemical potential will be fixed in the following by the two thermal baths. Note that this model is not equivalent to Anderson model [8] for which the hopping J_n is constant while the energy h_n of the fermion on each site is random.

The dynamics is governed by a Lindblad equation (1) with a non-local dissipator recently introduced for the homogeneous XX chain [23, 25]. Each subchain is coupled to a different bath. The latter are coupled to each eigenmodes k of the subchains via two Lindblad operators corresponding to the fermionic creation/annihilation operators $\eta^+_{\alpha,k}$ et $\eta_{\alpha,k}$. The dissipators read explicitly

$$D_\alpha[\rho] = 2\gamma \sum_k n_{\alpha,k}\Big(\eta^+_{\alpha,k}\rho\eta_{\alpha,k} - \frac{1}{2}\{\eta_{\alpha,k}\eta^+_{\alpha,k},\rho\}\Big) + 2\gamma\sum_k(1-n_{\alpha,k})\Big(\eta_{\alpha,k}\rho\eta^+_{\alpha,k} - \frac{1}{2}\{\eta^+_{\alpha,k}\eta_{\alpha,k},\rho\}\Big). \tag{10}$$

The constants $n_{\alpha,k}$ are fixed by the requirement that, in the absence of interchain coupling ($g = 0$), each subchain will thermalize independently. In the steady state, the average number of fermions in each mode is given by the Fermi-Dirac distribution:

$$\langle\eta^+_{\alpha,k}\eta_{\beta,k'}\rangle_{\rm st.} = n_{\alpha,k}\delta_{\alpha,\beta}\delta_{k,k'} = \frac{\delta_{\alpha,\beta}\delta_{k,k'}}{e^{(\varepsilon_{\alpha,k}-\mu_\alpha)/k_BT_\alpha}-1} \tag{11}$$

where T_α and μ_α are respectively the temperature and the chemical potential of the bath and $\varepsilon_{\alpha,k}$ is the energy of the k-th eigenmode of the isolated subchain. The dynamical equation of the equal-time correlation function $C_{\alpha,k;\beta,k'} = \langle\eta^+_{\alpha,k}(t)\eta_{\beta,k'}(t)\rangle$ can be cast into the convenient matrix form [23]

$$\frac{d}{dt}C = \frac{i}{\hbar}[W_0+W_1,C] - \{\Gamma,C\} + 2\mathcal{D} \tag{12}$$

where W_0, Γ and $\mathcal{D}$ are diagonal matrices whose entries are $\varepsilon_{\alpha,k}$, γ and $\gamma n_{\alpha,k}$ respectively. The non-diagonal matrix W_1 comes from the interchain coupling. In the following, Eq. (12) is integrated numerically using a 4th-order Runge-Kutta algorithm up to a time sufficiently large ($t = 100$) for the steady state to be reached.

The particle current between the two subchains reads [23]

$$\begin{aligned} J =& -ig\big(\langle c^+_{1,L}c_{2,1}\rangle - \langle c^+_{2,1}c_{1,L}\rangle\big) \\ =& \, 2g\Im\sum_{k,k'}V^*_{L,k}U_{1,k'}\langle\eta^+_{1,k}\eta_{2,k'}\rangle. \end{aligned} \tag{13}$$

In the steady state this current is equal to the current between the first subchain and the bath with which it is coupled:

$$J = -2\gamma\sum_k\big(n_{1,k} - \langle c^+_{1,k}c_{1,k}\rangle\big). \tag{14}$$

The particle current between the two subchains is measured numerically and averaged over all disorder configurations. The model will also be studied analytically in the limit of a weak interchain coupling g. To lowest order in g, the current (13) reads [23]

$$J = -4\gamma g^2\sum_{k,k'}|V_{k;L}|^2|U_{k';1}|^2\frac{\big(n_{2,k'}-n_{1,k}\big)}{4\gamma^2+\big(\varepsilon_{1,k}-\varepsilon_{2,k'}\big)^2} + \mathcal{O}(g^3) \tag{15}$$

The limit of an infinitely strong disorder, i.e. $r \to +\infty$, will be discussed.

3. Conductance between two pure subchains

We first consider two pure chains with $J_n = 1$. In the usual setup where the chain is coupled to two baths at its edges, the conductivity is infinite because the propagation of excitations (fermions) is ballistic. Any fermion of wavevector $k > 0$ injected in the system at the left boundary reaches the right boundary. In the system considered in this work, fermions introduced by the left bath into the left subchain can be scattered by the coupling between the two subchains:

$$-g(c^+_{1,L}c_{2,1} + c^+_{2,1}c_{1,L}) = -g\sum_{k,k'}\left(U_{kL}U^*_{k'1}\eta^+_{1,k}\eta_{2,k'} + U^*_{kL}U_{k'1}\eta^+_{2,k'}\eta_{1,k}\right) \tag{16}$$

and, as a consequence, reach the right subchain with a different wavevector. In a second step (second-order in g), they can be scattered back to the left subchain. The only constrain comes from the exclusion principle which forbids the scattering of an electron from the mode k in the left subchain to the mode k' in the right one if the latter is not unoccupied. Therefore, as in the Büttiker formalism, the total current (13) depends on the net number of allowed scattering channels from an occupied mode in one subchain to an unoccupied mode in the other subchain. Different chemical potentials in left and right reservoirs induce an imbalance and, as a consequence, a current.

Numerically, the current is observed to display a staircase-like behavior with the difference of chemical potentials $\Delta\mu$ between the two reservoirs at low temperature (figure 1). These steps are due to the quantization of the eigenmodes in the two finite-size subchains. They should not be confused with the steps observed in experiments [26, 27] where the wire is not purely one-dimensional so that the wavevectors have a transverse component which remains quantized when the length of the wire goes to infinity but not his width. In the model considered here, the steps are indeed observed to vanish as the length is increased (figure 2). As expected, the steps are smoothed as the temperature is increased. One can also notice by comparing the left and right figures 1 that J/g^2 displays only a small residual dependance on g when $g \leq 0.3$, in agreement with the perturbative expansion (15).

The conductance between two pure subchains can be computed analytically in some limits. As mentioned above, the coupling g is treated perturbatively. To lowest order in g, the current is given by (15) where $|V_{k;L}|^2 = |U_{k;1}|^2 = \frac{2}{L+1}\sin^2\frac{\pi k}{L+1}$, and $\varepsilon_{1,k} = \varepsilon_{2,k} = -2\cos\frac{\pi k}{L+1}$. Then, the temperature is set to zero for both left and right reservoirs and the dissipation γ is assumed to be strong. In these limits, the current reads

$$J \simeq -\frac{4g^2}{(L+1)^2\gamma}\sum_{k,k'=1}^{L}\sin^2\frac{\pi k}{L+1}\sin^2\frac{\pi k'}{L+1}\big(\theta(\mu_2 - \varepsilon_{2,k'}) - \theta(\mu_1 - \varepsilon_{1,k})\big). \tag{17}$$

Introducing the density of states on the first (or last) site of the chain as

$$\begin{aligned}\rho(\varepsilon) &= \frac{2}{L+1}\sum_k \delta(\varepsilon - \varepsilon_k)\sin^2\frac{\pi k}{L+1}\\ &\simeq \frac{2}{\pi}\int \delta(\varepsilon + 2\cos k)\sin^2 k dk\\ &= \frac{1}{\pi}\sqrt{1-\varepsilon^2/4}\end{aligned} \tag{18}$$

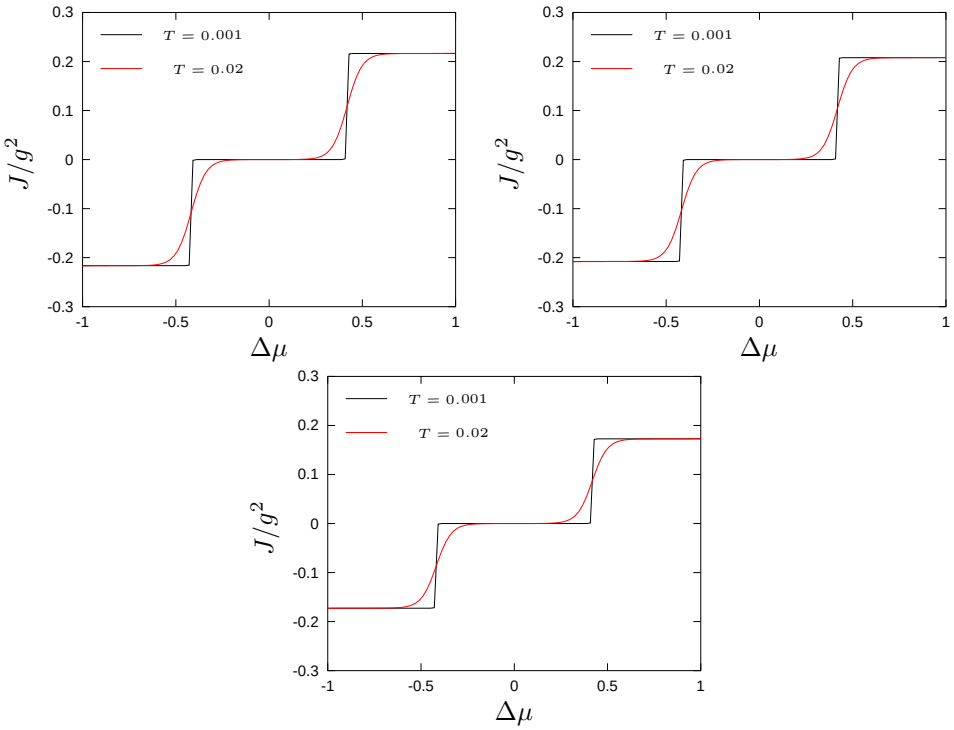

Figure 1. Current J/g^2 between two pure XX chains of size $L = 14$ versus $\Delta\mu$ when the two chains are in contact with baths at a different chemical potential $\Delta\mu/2$ and $-\Delta\mu/2$. The two curves corresponds to different temperatures $T = 0.001$ and $T = 0.02$. The interchain coupling is $g = 0.1$ (left), 0.3 (center), and 0.7 (right).

in the thermodynamic limit $L \to +\infty$, the current becomes

$$J \simeq -\frac{g^2}{\gamma}\int_{-2}^{2}\rho(\varepsilon)\rho(\varepsilon')\big(\theta(\mu_2-\varepsilon')-\theta(\mu_1-\varepsilon)\big)d\varepsilon d\varepsilon' \tag{19}$$

Swapping ε and ε' in the last term

$$J \simeq -\frac{g^2}{\gamma}\int_{\mu_1}^{\mu_2}\rho(\varepsilon')d\varepsilon'\int_{-2}^{2}\rho(\varepsilon)d\varepsilon, \tag{20}$$

the second integral is equal to 1. In the case $\mu_1 = \Delta\mu/2$ and $\mu_2 = -\Delta\mu/2$, the current finally reads

$$J \simeq \frac{g^2}{\pi\gamma}\int_{-\Delta\mu/2}^{\Delta\mu/2}\sqrt{1-\varepsilon^2/4}d\varepsilon = \frac{g^2}{\pi\gamma}\left(\frac{\Delta\mu\sqrt{16-\Delta\mu^2}}{8}+2\arcsin\frac{\Delta\mu}{4}\right) \tag{21}$$

In the neighborhood of $|\Delta\mu| = 0$, the current behaves as $J \simeq \frac{g^2}{\pi\gamma}\Delta\mu$, i.e. the conductance is $\frac{g^2}{\pi\gamma}$. Despite the various assumptions made, the behavior Eq. (21) is consistent with the numerical data (figure 2), even at non-zero temperature and for relatively small lattice sizes.

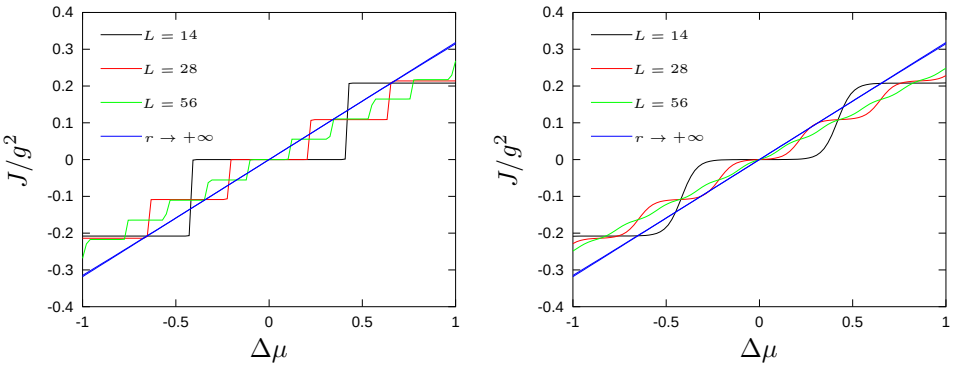

Figure 2. Current J/g^2 between two pure XX chains versus $\Delta\mu$ when the two chains are in contact with baths at a different chemical potential $\Delta\mu/2$ and $-\Delta\mu/2$. The different curves correspond to different lattice sizes L and, the last one, to the analytical expression (21). On the left graph, the temperature of the left and right baths is $T = 0.001$ while it is equal to 0.02 on the right.

4. Conductance between a pure and a random system

4.1. Conductance at zero chemical potential

The right chain is still homogeneous ($J = 1$) but the left one is now random with $J_n \in \{r, 1/r\}$. The temperatures of the two baths are equal but the chemical potentials are assumed to be $\Delta\mu/2$ for the left bath and $-\Delta\mu/2$ for the right one. The average current $\bar{J}$ is plotted on figure 3. As in the pure case considered above, no current flows between the two subchains if $\Delta\mu = 0$. For the weakest disorder ($r = 2$), the curve displays a shape still roughly similar to the pure case (figure 1). However, as the strength of disorder increases, the curve becomes steeper and steeper at $\Delta\mu = 0$. The conductance, defined as the derivative [5]

$$G = \left(\frac{d\bar{J}}{d\Delta\mu}\right)_{\Delta\mu=0}, \tag{22}$$

increases with r. From the curve corresponding to the strongest disorder ($r = 10$), one can conjecture that a gap will open at zero temperature in the limit of infinite randomness, yielding in this case an infinite conductance. Both finite disorder and zero-temperature smooth the curve and make the conductance finite.

The current being related to the imbalance between the number of scattering channels from left to right and right to left, an explanation for the opening of a gap observed numerically should be looked for in the energy spectrum of the random XX subchain. As often noticed in the literature, the level spacing distribution of the random XX subchain is not compatible with the Gaussian Orthogonal Ensemble observed in chaotic systems [28, 29]. It can be checked numerically that the levels are distributed according to a Poisson distribution $\wp(\Delta E) \sim e^{-\Delta E}$ in the random XX chain. However, this distribution is not relevant to our purpose because the current is expressed in terms of fermionic excitations. More relevant here is the density of states of the free fermion gas after the Jordan-Wigner transform of the XX model. The latter is presented on figure 4. For strong randomness, the density of states appears as a sequence of Dirac peaks, the largest one being located at $\varepsilon = 0$. This

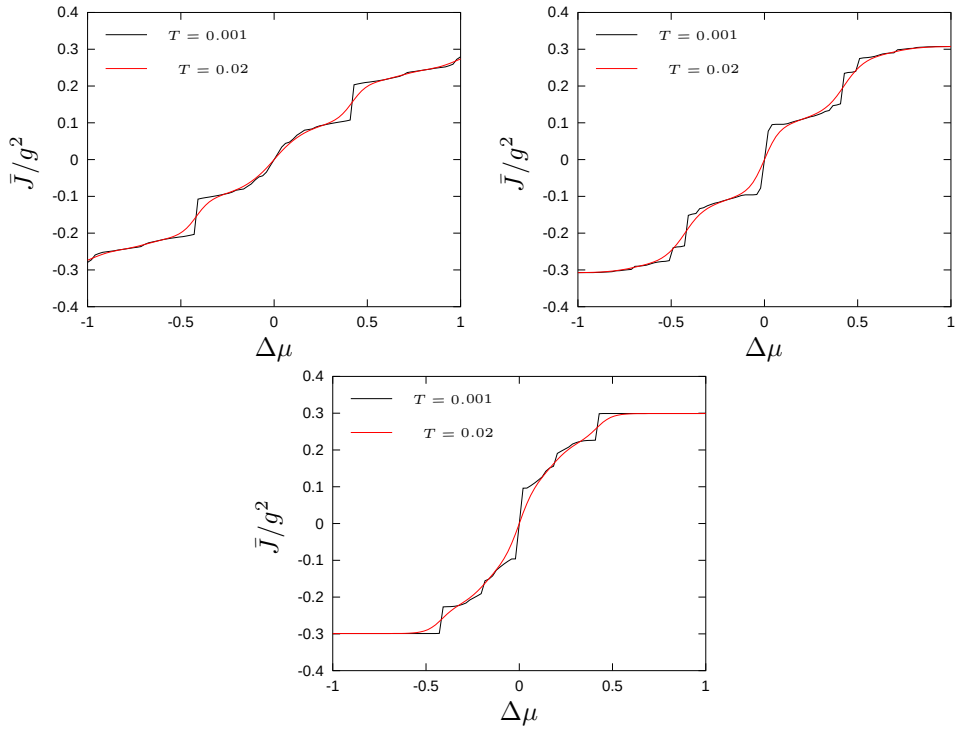

Figure 3. Average current $\bar{J}/g^2$ between a random and a pure XX chains of size $L = 14$ versus $\Delta\mu$ when the two chains are in contact with baths at different chemical potentials $\Delta\mu/2$ and $-\Delta\mu/2$. The couplings of the random XX model are randomly chosen in $\{1/r; r\}$ with $r = 2$ (left), $r = 4$ (center) and $r = 10$ (right). The two curves corresponds to different temperatures $T = 0.001$ and $T = 0.02$.

behavior is easily understood in the infinite-randomness limit $r \to +\infty$. For a given disorder realization, the fermion Hamiltonian is a tridiagonal matrix whose elements are $H_{n,n+1} = H_{n+1,n} = J_n$ where J_n is a random variable in $\{r, 1/r\}$. In the infinite-randomness limit $r \to +\infty$, at least one fourth of the eigenvalues of the Hamiltonian are expected to vanish. Indeed, the probability that two consecutive couplings, say J_n and J_{n+1}, are both equal to $1/r$, and therefore vanish in the limit $r \to +\infty$, is $1/4$. As a consequence, the $(n+1)$-th line of the matrix $H - \varepsilon$ has only one non-zero element, $-\varepsilon$ on the diagonal. The determinant of the $L \times L$ matrix $H - \varepsilon$ therefore reads $(-\varepsilon)M_{n+1,n+1}$ where $M_{n+1,n+1}$ is the minor of the matrix. The characteristic polynomial of the matrix can be factorized by $-\varepsilon$ which implies that $\varepsilon = 0$ is one of its roots. When N consecutive couplings are large and bounded by two weak couplings, i.e. $J_n = J_{n+N+1} = 1/r$ and $J_{n+m} = r$ for any $m = 1, \ldots, N$, the $N+1$ sites $n+1$ to $n+N+1$ are uncoupled from the rest of the system in the infinite-randomness limit. For a given disorder realization, the fermion Hamiltonian is a block diagonal matrix. Each block of N large couplings corresponds to the Hamiltonian of a fermion on a chain of $N+1$ sites with a hopping constant r. The $N+1$ eigenvalues are [30]

$$\varepsilon_{N,q} = -2r \cos \frac{\pi q}{N+2}, \quad q = 1, \ldots, N+1 \tag{23}$$

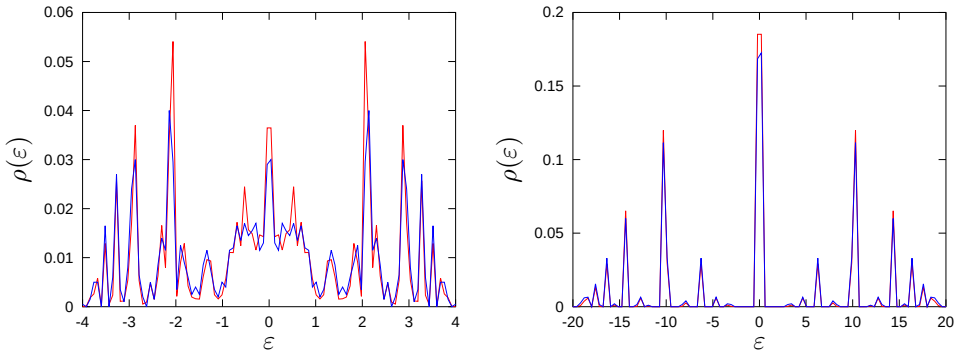

Figure 4. Probability density $\wp(\varepsilon)$ of the eigenvalues of the random tight-binding Hamiltonian with $r = 2$ (left) and $r = 10$ (right). The red curve corresponds to the distribution for a lattice size $L = 16$ averaged over the 32768 random configurations of the couplings. The blue curve is the probability density for a single random realization of a large lattice of size $L = 2000$.

and the associated eigenvectors

$$\phi_{N,q}(m) = \sqrt{\frac{2}{N+2}} \sin \frac{\pi q m}{N+2}, \quad m = 1, \ldots, N+1. \tag{24}$$

The eigenvectors have zero component on other sites. The probability to observe such a block is $1/2^{N+2}$, i.e. the localization length is $\xi = 1/\ln 2$. The density of states is not a smooth function, even in the thermodynamic limit, but displays a discrete number of peaks. Each one of these peaks can be associated to two numbers, $N \in \mathbb{N}$ and $q = 1, \ldots, N+1$. This picture is consistent with what is observed numerically on figure 4.

Coming back to the expression (15) of the current, one can notice that the scattering of an eigenmode k of the left subchain to an eigenmode k' of the right one is weighted by $|V_{k;L}|^2 |U_{k';1}|^2$, i.e. the probability to find the fermion in the eigenmode k on site L of the left subchain times the probability to find the fermion in the eigenmode k' on site 1 of the right one. Since the eigenmodes of the pure right subchain are delocalized, $|U_{k';1}|^2 = \frac{2}{L+1} \sin^2 \frac{\pi k'}{L+1}$ does not vanish. In contrast, in the random left subchain, all states are localized in the thermodynamic limit. Therefore, only those states with a non-zero probability on the site L will contribute to the current. These states are surface states and were not discussed above. If the last coupling $J_{L-1} = 1/r$ is weak then, in the infinite-randomness limit, the site L is decoupled from the rest of the chain. All elements $H_{L,n}$ of the Hamiltonian vanish. Therefore, there exists an eigenvalue $\varepsilon = 0$ associated to the eigenvector $\phi(n) = \delta_{n,L}$. The probability of such an event is $1/2$. In a way analogous to what happens in the bulk, when the N last couplings are equal to r, i.e. $J_{L-N} = \ldots = J_{L-1} = r$ and $J_{L-N-1} = 1/r$, then, in the infinite-randomness limit, the last $N+1$ sites are decoupled from the rest of the system. A $(N+1) \times (N+1)$ block appears on the diagonal of the Hamiltonian. After diagonalization, the $N+1$ eigenvectors are found to be given by (24) with the associated energies (23). The probability of such a block is $1/2^{N+1}$.

At zero-temperature, the average current reads

$$\bar{J} = -4\gamma g^2 \sum_{k,k'} \overline{|V_{k;L}|^2 |U_{k';1}|^2 \frac{\theta(\mu_2 - \varepsilon_{2,k'}) - \theta(\mu_1 - \varepsilon_{1,k})}{4\gamma^2 + \left(\varepsilon_{1,k} - \varepsilon_{2,k'}\right)^2}} + \mathcal{O}(g^3). \tag{25}$$

All energies $\varepsilon_{1,k}$ (23) are proportional to r, and therefore diverge in the infinite-randomness limit, apart from the surface states for which $\varepsilon = 0$. As a consequence, only those latter states contribute to the current (25). The energies $\varepsilon_{N,q}$ vanish when the fermion is localized on the site L of the left chain or in a block of N strong couplings when N is even and $q = \frac{N}{2} + 1$. The square of the wavefunction on the right site, i.e. $|V_{k;L}|^2$, is equal to one in the former case and to

$$|\phi_{N,q=\frac{N}{2}+1}(N)|^2 = \frac{2}{N+2} \sin^2\left(\frac{\pi N q}{N+1}\right) = \frac{2}{N+2} \tag{26}$$

in the latter. The probability of such a block being $1/2^{N+1}$, the weight appearing in the current is

$$\frac{1}{2} + \sum_{\substack{N=2 \\ \text{even}}}^{+\infty} \frac{|\phi_{N,q=\frac{N}{2}+1}(N)|^2}{2^{N+1}} = \frac{1}{2} + \sum_{\substack{N=2 \\ \text{even}}}^{+\infty} \frac{1}{(N+2)2^N} = 2 \ln \frac{4}{3}. \tag{27}$$

The average current is now

$$\bar{J} = -8\gamma g^2 \ln \frac{4}{3} \sum_{k'} \frac{2}{L+1} \sin^2\left(\frac{\pi k'}{L+1}\right) \frac{\theta(\mu_2 - \varepsilon_{2,k'}) - \theta(\mu_1)}{4\gamma^2 + (\varepsilon_{2,k'})^2} + \mathcal{O}(g^3). \tag{28}$$

The sum is evaluated in the thermodynamic limit $L \to +\infty$. When $\mu_1 < 0$, the left states $\varepsilon_1 = 0$ are empty so the current flows from the right to the left:

$$\begin{aligned} \bar{J}(\mu_2) = & -\frac{16\gamma g^2}{\pi} \ln \frac{4}{3} \int_0^{k_F} \frac{\sin^2 k}{4\gamma^2 + 4\cos^2 k} dk \quad (\mu_1 < 0) \\ = & -\frac{4\gamma g^2}{\pi} \ln \frac{4}{3} \left[\frac{\sqrt{1+\gamma^2}}{\gamma} \arctan \frac{\gamma \tan k_F}{\sqrt{1+\gamma^2}} - k_F \right] \end{aligned} \tag{29}$$

where the Fermi wavevector satisfies $-2\cos k_F = \mu_2$ and the $\arctan(x)$ function should be defined on $[0;\pi[$ instead of $]-\pi/2;\pi/2[$. When $\mu_1 > 0$, the right states are occupied and the current flows only from left to right:

$$\bar{J}(\mu_2) = \frac{4\gamma g^2}{\pi} \ln \frac{4}{3} \left[\frac{\sqrt{1+\gamma^2}}{\gamma} \arctan \frac{\gamma \tan k}{\sqrt{1+\gamma^2}} - k \right]_{k_F}^{\pi} \quad (\mu_1 > 0) \tag{30}$$

Considering as before $\mu_1 = \Delta\mu/2$ and $\mu_2 = -\Delta\mu/2$, the current turns out to be an odd function of $\Delta\mu$ and to display a quasi-linear dependance on $\Delta\mu$ when $\Delta\mu \sim \mathcal{O}(1)$ but with a gap at $\Delta\mu = 0$ equal to

$$\Delta\bar{J} = 4\gamma g^2 \ln \frac{4}{3} \left(\frac{\sqrt{1+\gamma^2}}{\gamma} - 1 \right) \tag{31}$$

Since the derivative of (29) is

$$\frac{d\bar{J}}{dk_F} = \frac{4\gamma g^2}{\pi} \ln \frac{4}{3} \frac{\tan^2 k_F}{1 + \gamma^2 + \gamma^2 \tan^2 k_F} \tag{32}$$

the slope of the current at small non-zero chemical potential is given by

$$\lim_{k_F \to \pi/2^+} \frac{d\bar{J}}{dk_F} \frac{dk_F}{d\Delta\mu} = \frac{4\gamma g^2}{\pi} \ln \frac{4}{3} \times \frac{1}{\gamma^2} \times \frac{1}{4} \tag{33}$$

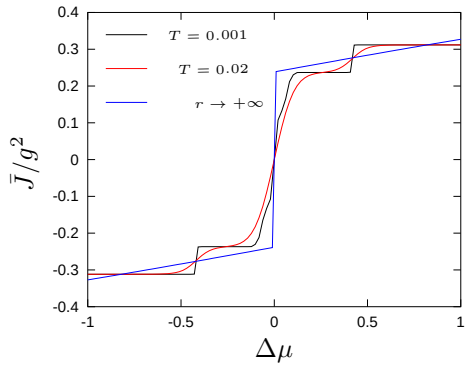

Figure 5. Average current $\bar{J}/g^2$ between a random and a pure XX chain of sizes $L = 14$ versus $\Delta\mu$ when the two chains are in contact with baths at a different chemical potentials $\Delta\mu/2$ and $-\Delta\mu/2$. The couplings of the random XX model are randomly chosen in $\{1/r; r\}$ with $r = 30$ and the inter-chain coupling is $g = 0.1$. The two first curves correspond to different temperatures $T = 0.001$ (black) and $T = 0.02$ (red). The last curve (blue) is the analytical expression (29) and (30).

when $\Delta\mu > 0$. Repeating the calculation for $\Delta\mu < 0$, it follows that the average current at first order in $\Delta\mu$ is

$$\bar{J} = \frac{g^2}{\gamma\pi} \ln\frac{4}{3}\Delta\mu + 2\gamma g^2 \ln\frac{4}{3}\left(\frac{\sqrt{1+\gamma^2}}{\gamma} - 1\right) \text{ sign } \Delta\mu + \mathcal{O}(\Delta\mu^2). \tag{34}$$

When plotted on figure 5, this expression cannot be distinguished from equations (29) and (30). The first term is similar to the linear behavior observed in the pure case. The slope $\bar{G} = \frac{g^2}{\gamma\pi} \ln\frac{4}{3}$ only differs from the conductance of the pure chain by a factor $\ln\frac{4}{3}$. However, the second term of (34) leads to an infinite conductance at zero chemical potential in the infinite-randomness limit.

4.2. Conductance at non-zero chemical potential

In the pure case, the current J between the two subchains vanishes when the chemical potentials of the two baths are equal. This is no longer the case when one of the chains is random. Instead, a non-zero current is observed whenever the chemical potential in the random subchain is different from zero. On figures 6, the average current $\bar{J}(\mu_1, \mu_2)$, as given by equations (29) and (30) in the infinite-randomness limit, is plotted versus the chemical potentials μ_1 and μ_2 of the two baths in contact with the two subchains. The current displays a monotonous dependance on μ_2 but depends only on the sign of μ_1. As discussed in the previous section in the case $\mu_2 = 0$, a discontinuity is observed at $\mu_1 = 0$, leading to an infinite conductance.

Even though the current does not vanish when $\mu_1 \neq 0$, a conductance can still be defined as the linear response of the system to an imbalance of the chemical potentials of the two baths. Considering now the setup where $\mu_1 = \mu + \Delta\mu/2$ and $\mu_2 = \mu - \Delta\mu/2$, the average conductance is assumed to be

$$\bar{G}(\mu) = \left(\frac{d\bar{J}}{d\Delta\mu}\right)_{\Delta\mu=0}. \tag{35}$$

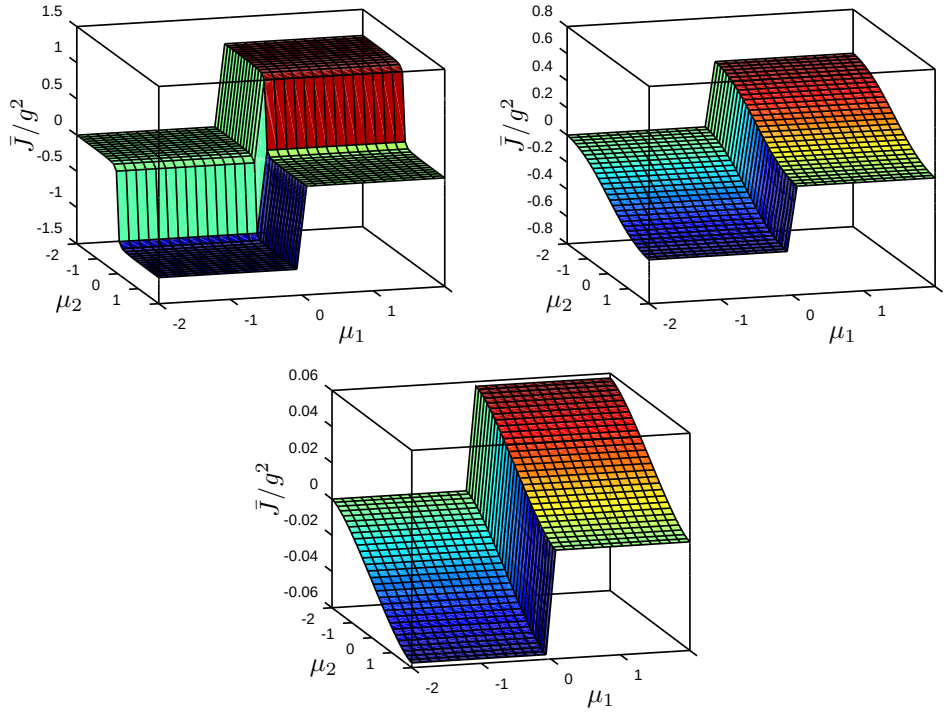

Figure 6. Average current $\bar{J}/g^2$ versus the chemical potentials of the two reservoirs in the infinite-randomness limit. The graphs correspond to different values of the dissipation of the baths: $\gamma = 0.01$ (left), $\gamma = 1$ (center), and $\gamma = 10$ (right).

Numerically, this quantity was computed by approximating the derivative with a linear difference:

$$\bar{G}(\mu) \simeq \frac{\bar{J}(\mu + \Delta\mu/2, \mu - \Delta\mu/2) - \bar{J}(\mu, \mu)}{\Delta\mu} \tag{36}$$

with the small value $\Delta\mu = 10^{-4}$. The numerical data are presented on figures 7. Due to the discreteness of the spectrum of the pure subchain, the conductance displays peaks which become sharper and sharper as the strength of disorder increases. Such a configuration of peaks is not a specificity of random chains. It is also observed in pure XX chains (see in particular figure 4 of Ref. [23]). However, in the random case, the height of the peak centered at $\mu = 0$ diverges as the strength of disorder increases while all other peaks remain finite. This behavior is understood in the infinite-randomness limit. Using Eq. (32), the average conductance is found to be

$$\bar{G}(\mu) = \frac{\gamma g^2}{\pi} \ln \frac{4}{3} \frac{\tan^2 k_F}{1 + \gamma^2 + \gamma^2 \tan^2 k_F} \frac{1}{\sin k_F} + 4\gamma g^2 \ln \frac{4}{3} \left(\frac{\sqrt{1+\gamma^2}}{\gamma} - 1 \right) \delta(\mu) \tag{37}$$

where $\mu = -2 \cos k_F$. The Dirac distribution at zero chemical potential discussed in the previous section has been added to the derivative. Eliminating k_F, the expression

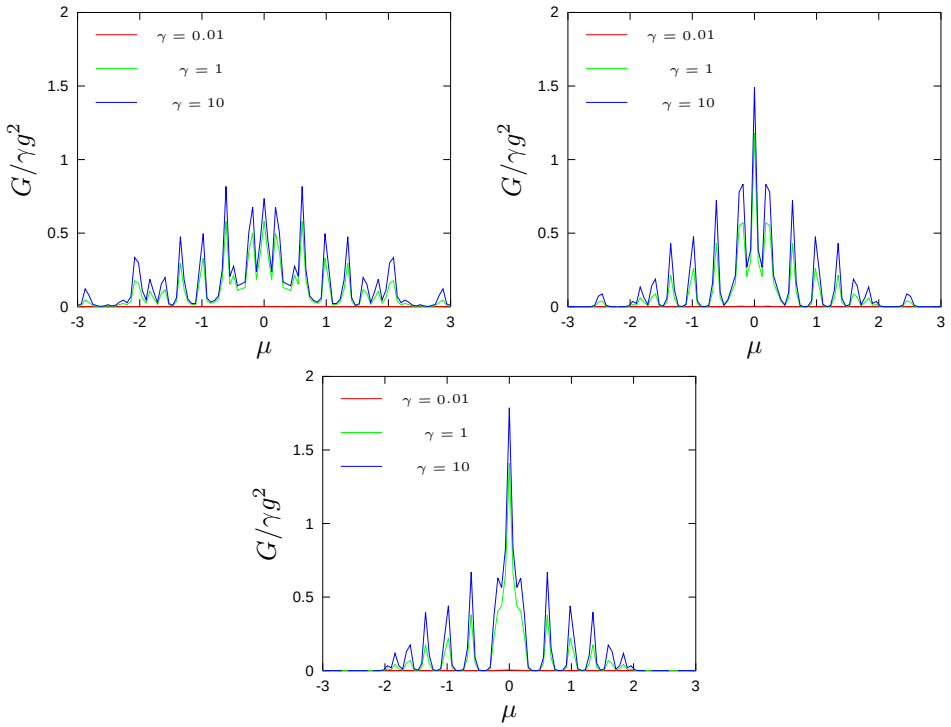

Figure 7. Average conductance $\bar{G}(\mu)/\gamma g^2$ between a random and a pure XX chains of size $L = 14$ versus the chemical potential μ when the two chains are in contact with baths at a different chemical potentials $\mu + \Delta\mu/2$ and $\mu - \Delta\mu/2$ where $\Delta\mu = 10^{-4}$. The couplings of the random XX model are randomly chosen in $\{1/r; r\}$ with $r = 2$ (left), $r = 4$ (center) and $r = 10$ (right). The different curves corresponds to different values of the dissipation γ. The temperature is $T = 0.02$.

can be simplified to

$$\bar{G}(\mu) = \frac{\gamma g^2}{\pi} \ln \frac{4}{3} \frac{4-\mu^2}{4\gamma^2+\mu^2} \frac{1}{\sqrt{1-\mu^2/4}} + 4\gamma g^2 \ln \frac{4}{3} \left(\frac{\sqrt{1+\gamma^2}}{\gamma} - 1 \right) \delta(\mu). \tag{38}$$

The average conductance is plotted on figure 8. Though similar to the one obtained in the pure case when $\gamma = 1$, the curve $\bar{G}(\mu)$ versus μ is significantly different at low dissipation, i.e. $\gamma \ll 1$. Since randomness limits the number of channels from one subchain to the other, a low coupling γ with the bath restricts the conductance to a small window around $\mu = 0$.

5. Conclusions

A model consisting in two XX chains, one with random couplings drawn from a binary distribution and the second one homogeneous, has been considered. The two chains are coupled to different thermal baths through a non-local Lindblad dissipator and connected by their edges. Despite the fact that all eigenstates in the random subchain are localized, a current is induced between the two subchains in the steady state

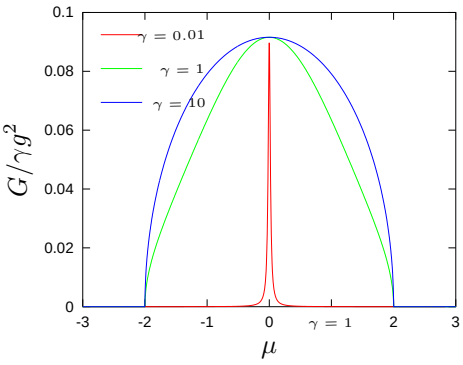

Figure 8. Average conductance $\bar{G}(\mu)/\gamma g^2$ when the chemical potentials of the two reservoirs are $\mu \pm \Delta\mu/2$ versus μ in the infinite-randomness limit. The different curves corresponds to different values of the dissipation γ. Note that the Dirac peak at $\mu = 0$ has not been plotted.

because of the non-locality of the dissipator. A divergence of the conductance is observed at zero chemical potential as the disorder strength increases and is explained in terms of the density of states of the localized states of the random subchain.

As far as we are aware, such a diverging conductance has not been observed before in random quantum systems. Our model has indeed several peculiarities. As mentioned above, the coupling to the baths is non-local while boundary dissipators are usually considered. Then, most studies on Anderson localization are based on tight-binding models with random local energies rather than random hopping constants. Moreover, these random energies are usually distributed according to a Gaussian law or a uniform law. The binary distribution of the hopping couplings is a crucial ingredient for the divergence of the conductance.

Nevertheless, the model consider in this study is not completely unrealistic. Besides experimental realizations of spin chains, one can imagine long polymers made of two kinds of monomer with different electrical conductivities and adsorbed on a metallic surface that could play the role of a reservoir.

Acknowledgements

The authors gratefully thanks Pedro Guimarães for having presented him his work [23] during the MECO conference in Lyon.

References

[1] Fisher D S, 1992 *Phys. Rev. Lett.* **69** 534 ; Fisher D S, 1995 *Phys. Rev. B* **51** 6411
[2] Iglói F, and Monthus C, 2005 *Phys. Rep.* **412** 277
[3] Motrunich O, Damle K, and Huse D A, 2001 *Phys. Rev. B* **63**, 134424
[4] Antal T, Rácz Z, Rákos A, and Schütz G M, 1999 *Phys. Rev. E* **59**, 4912
[5] Landauer R, 1957 *IBM J. Res. Dev.* **1** 223 ; Landauer R 1970 *Phil. Mag.* **21** 863
[6] S. Datta, 1995 *Electronic Transport in Mesoscopic Systems* Cambridge University Press, Cambridge
[7] Kawabata A, 2007 *Rep. Prog. Phys.* **70** 219
[8] Anderson P W, 1958 *Phys. Rev.* **109** 1492
[9] Kramer B and MacKinnon A, 1993 *Rep. Prog. Phys.* **56** 1469

[10] Evers F and Mirlin A D, 2008 *Rev. Mod. Phys.* **80**, 1355
[11] Basko D, Aleiner I, and Altshuler B, 2006 *Annals of Physics* **321**, 1126
[12] Bertini B, Collura M, de Nardis J, and Fagotti M, 2016 *Phys. Rev. Lett.* **117** 207201
[13] Karevski D, Platini T, 2009 *Phys. Rev. Lett.* **102** 207207
[14] Breuer H P, and Petruccione F, 2002 *The theory of open quantum systems* Oxford University Press
[15] Lindblad G, 1976 *Commun. Math. Phys.* **48** 119
[16] Karevski D and Platini T, 2009 *Phys. Rev. Lett.* **102** 207207
[17] Žnidarič M, 2010 *J. Phys. A: Math. Theor.* **43** 415004
[18] Karevski D, Popkov V, Schütz G, 2013 *Phys. Rev. Lett.* **110** 047201
[19] Galperin M, Ratner M A, and Nitzan A, 2007 *J. Phys.: Condens. Matter* **19** 103201
[20] Žnidarič M, and Horvat M, 2013 *Eur. Phys. J. B* **86** 67
[21] Monthus C, 2017 *J. Stat. Mech.* 043302
[22] Yusipov I, Laptyeva T, Denisov S, and Ivanchenko M, 2017 *Phys. Rev. Lett.* **118**, 070402
[23] Guimarães P H, Landi G T, and de Oliveira M J 2016 *Phys. Rev. E* **94** 032139
[24] Schulz P A, Galvo D S, and Caldas M J, 1991 *Phys. Rev. B* **44** 6073
[25] Santos J P, and Landi G T, 2016 *Phys. Rev. E* **94** 062143
[26] van Wees B J, van Houten H, Beenakker C W J, Williamson J G, Kouwenhoven L P, van der Marel D, and Foxon C T 1988 *Phys. Rev. Lett.* **60** 848
[27] Wharam D A, Thornton T J, Newbury R, Pepper M, Ahmed H, Frost J E F, Hasko D G, Peacock D C, Ritchie D A, and Jones G A C, 1988 *J. Phys. C* **21** L887
[28] Bohigas O, Giannoni M J, and Schmit C 1984 *Phys. Rev. Lett.* **52** 1
[29] Beenakker C W J, 1997 *Rev. Mod. Phys.* **69** 731
[30] Nechaev S, 2017, `arXiv:1705.08013`